# A negative-thermal-quenching $LaMgAl_{11}O_{19}$: $Er^{3+}$, $Sm^{3+}$ phosphor achieved by energy transfer from $Er^{3+}$ to $Sm^{3+}$

**Xin Min,*[1, 2] Cheng-Yen Lao,[2] Yifei Liu,[1] Haipeng Ji,[3] Xiaowen Wu,[1] Yan'gai Liu,[1] Zhaohui Huang,[1] Minghao Fang,*[1] Amr. M. Abdelkader,[4] Ramachandran Vasant Kumar[2], Kai Xi *[5]**

[1] Beijing Key Laboratory of Materials Utilization of Nonmetallic Minerals and Solid Wastes, National Laboratory of Mineral Materials, School of Materials Science and Technology, China University of Geosciences (Beijing), Beijing, 100083, P. R. China. [2] Department of Materials Science and Metallurgy, University of Cambridge, Cambridge, CB3 0FS, UK. [3] School of Materials Science and Engineering, Zhengzhou University, Zhengzhou, 450001, P. R. China. [4] Faculty of Science and Technology, Bournemouth University, Talbot Campus, Fern Barrow, Poole, BH12 5BB, England. [5] Department of Applied Chemistry, School of Chemistry, University Engineering Research Center of Energy Storage Materials and Chemistry of Shaanxi Province, State Key Laboratory for Electrical Insulation and Power Equipment, Xi'an Jiaotong University, Xi'an 710049, China. *Correspondence should be addressed to X.M. (email: minx@cugb.edu.cn) or to M.F. (email: fmh@cugb.edu.cn) or to K. X. (email: kx210.cam@xjtu.edu.cn).

**Abstract:**

Phosphor-converted white light-emitting diodes (pc-wLEDs) are drawing ever-increasing attention towards electronic applications. However, thermal quenching, the intensity decay with increasing temperature, presents a significant challenge for high power operation. We reverse the effect with a negative-thermal-quenching property based on energy transfer from one luminescent center to another center. The $LaMgAl_{11}O_{19}$: $Er^{3+}$, $Sm^{3+}$ (LMA: $LaMgAl_{11}O_{19}$: $Er^{3+}$, $Sm^{3+}$) phosphor has been designed, which shows a positive relationship between emission intensity and operating temperature up to 573 K (300 °C). As the temperature rises, energy transfer from $Er^{3+}$ to $Sm^{3+}$ occurs with higher efficiency because of stronger ionic vibration. As a result, the phosphor luminescence intensity at elevated temperatures is enhanced. Our design for negative-thermal quenching phosphor laid the foundation for the research of high-power pc-wLEDs or lasers at higher temperatures. It also has potential for wide-temperature-sensing-range radiometric optical thermometry applications.

**Keywords:** negative-thermal-quenching; energy transfer; phosphors; wLEDs

## 1. Introduction

Phosphor-converted white light-emitting diodes (pc-wLEDs) are considered the next-generation solid-state lighting due to low energy consumption, high reliability and luminous efficiency, long lifetime and environmentally friendly characteristics [1-4]. Combining single-phased trichromatic phosphors with ultraviolet (UV) LED chips is becoming particularly important for generating white light [5-7]. LED demonstrates excellent color rendering indexes, minor color aberration, and high luminous efficiency. However, the emission intensity usually deteriorates during high-power operation because of the nonradiative relaxation of electrons from an excited state to the ground state at temperatures higher than 423 K [8-10]. This emission thermal quenching (TQ) behavior plagues the efficiency and color rendering index [11, 12]. Therefore, in order to improve the luminous efficiency of white LED at high temperature, it is necessary to carry out further research.

Previous research shows TQ depends mainly on the structural rigidity of the host materials [13-17]. A rigid bonding network and high bond strength can substantially minimize the emission loss with increasing temperature [18-20]. Many researchers have reported that ion-doping-induced defects can effectively mitigate TQ [21, 22]. Due to the energy compensation of zinc vacancies and the existence of oxygen vacancy defects, Li et al. reported an anti-thermal-quenching cyan-emitting $Ba_2ZnGe_2O_7:Bi^{3+}$ phosphor, the emission intensity of the phosphor at 150 °C is 114 % of that at room temperature[23]. Wu et al. reported a $Sm^{3+}$ and $Eu^{3+}$ co-doped $SrBi_2B_2O_7$ phosphors, according to the crystal local environment research and first-principles calculation, the crystal structure of $SrBi_2B_2O_7$: $Sm^{3+}$, $Eu^{3+}$ is more compact at high temperature. Therefore, the formation energy of the defects is low, which enhanced the thermal stability of the phosphor[24]. Wang et al. reported a $Ca_{3.6}In_{3.6}(PO_4)_6:Sm^{3+}$, $Eu^{3+}$ phosphor with an internal quantum efficiency of up to 82.8 %, double ion co-doping increases the local symmetry of the crystal. During the energy transfer process from $Sm^{3+}$ to $Eu^{3+}$, the synergistic enhancement of thermal stability of phosphors was realized[25]. In particular, recent studies have shown that the zero-thermal-quenching phenomenon at elevated temperature can occur with the $Na_{3-2x}Sc_2(PO_4)_3:xEu^{2+}$ phosphor through the migration of thermally reactivate defect-trapped electrons to the conductive bandgap of $Eu^{2+}$ [26]. These results indicate the role of electron transfer in optimizing the design of phosphors with excellent thermal behavior. However, controlling the level of the defects and the reactivation process is practically challenging (Fig. 1).

Energy transfer from a sensitized center to a luminescent center, which is also implemented through electron migration, is a common approach to designing emission-tunable single-phased phosphors for wLEDs [27-29]. Here, we firstly design the energy transfer process from $Er^{3+}$ to $Sm^{3+}$ and prepare a color-tunable and negative-thermal-quenching phosphor LMA: $Er^{3+}$, $Sm^{3+}$ with stable color rendering at increasing temperatures, based on the absolute overlap between the UV activated emission spectra of $Er^{3+}$ and the adsorption spectra of $Sm^{3+}$ in LMA host. The design reverses the TQ with rising emission intensity up to 573 K achieved by the energy transfer process. The unique luminescence properties of LMA: $Er^{3+}$, $Sm^{3+}$ confirmed that the energy transfer is an effective tactic for designing novel phosphors with the enhanced thermal property.

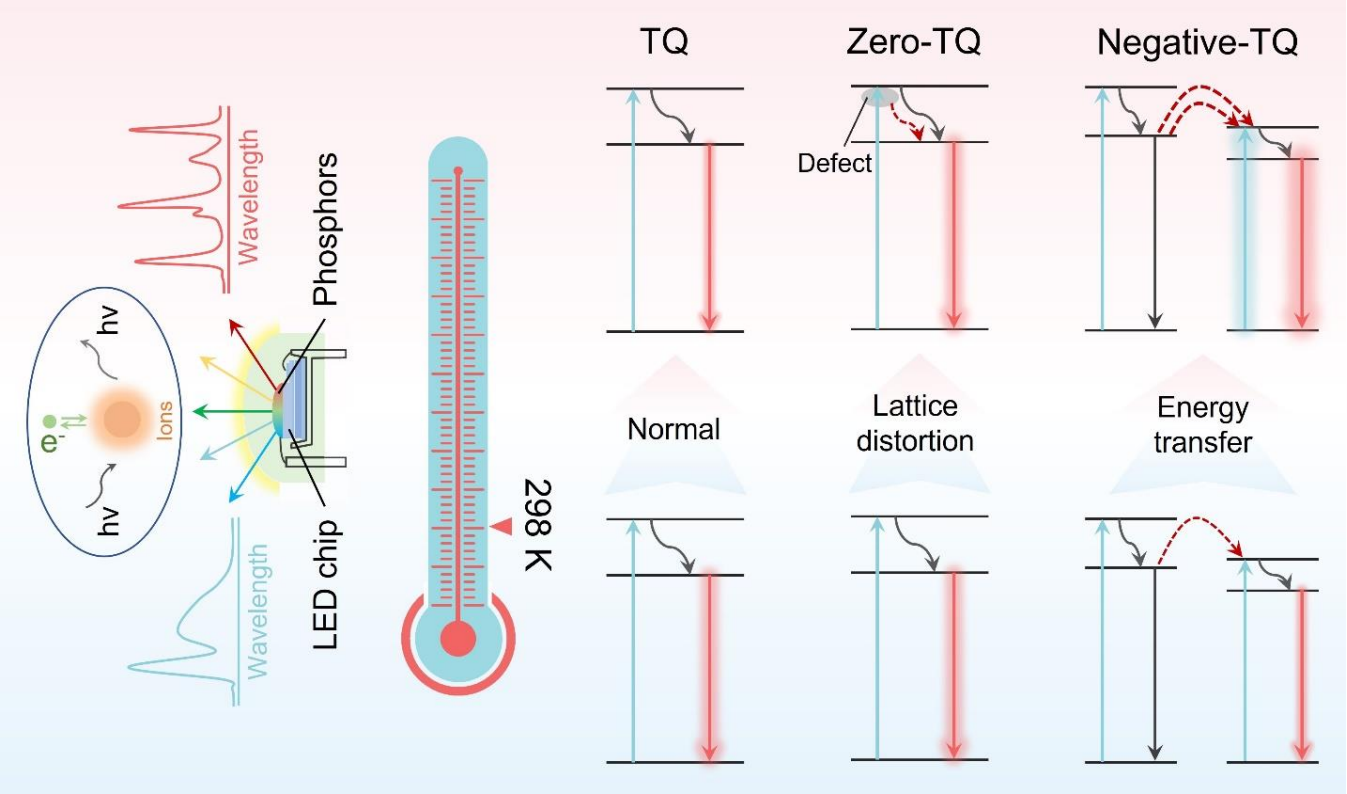


**Fig. 1. Schematic illustration of the thermal quenching effect of pc-wLEDs.** The left part shows the schematic of the pc-wLED device. The right part shows the mechanisms of the normal TQ, zero-TQ, and negative TQ effect of phosphors at high temperatures. The thickness of the outline during the conversion process depicts the extent of luminous intensity.

## 2. Experimental Section

### 2.1 Materials and Synthesis

All phsphors investigated in this paper including LMA: $x\mathrm{Er}^{3+}$ ($x$=0.01, 0.03, 0.05, 0.08, 0.1, 0.15), LMA: $0.08\mathrm{Sm}^{3+}$, and LMA: $0.1\mathrm{Er}^{3+}$, $y\mathrm{Sm}^{3+}$ ($y$=0.01, 0.03, 0.05, 0.08, 0.1, 0.2) were prepared via a high temperature solid state reaction method. Analytical grad $La_2O_3$ (99.99%), $Mg(OH)_2$ (99.9%), $Al(OH)_3$ (99.9%), $Er_2O_3$ (99.99%), and $Sm_2O_3$ (99.99%) were used as raw materials, weighed quickly, and mixed in an agate mortar for about 30 min. Then the mixtures were charged into an alumina crucible, calcined at 1600 °C for 4 h, and finally ground into powders after natural cooling for further measurements.

### 2.2 Characterization

The phase composition for the phosphor samples was investigated by x-ray diffraction (XRD, D8 Advance diffractometer, Bruker Corporation, Germany) with a Cu Kα (λ=1.5406 Å) radiation. The powder XRD pattern for Rietveld analysis of LMA: $0.1\mathrm{Er}^{3+}$, $0.08\mathrm{Sm}^{3+}$ was collected at a step size of 0.02° and 20 s counting time per step. The Rietveld refinement was analyzed by TOPAS 4.2, using magnetoplumbite-type structure LMA as the starting structure [30]. The morphologies and elemental analysis of the LMA: $0.1\mathrm{Er}^{3+}$, LMA: $0.08\mathrm{Sm}^{3+}$, and LMA: $0.1\mathrm{Er}^{3+}$, $0.08\mathrm{Sm}^{3+}$ phosphors were studied using a Field-emission scanning electron

microscope (FESEM, SUPRA 55, Zeiss, Germany) equipped with energy-dispersive X-ray spectroscopy (EDS). A transmission electron microscope (TEM/HRTEM, JEM-2100HR, JEOL, Japan) was used to obtain the microstructure of the as-prepared samples. The photoluminescence excitation (PLE) and emission (PL) spectra at room temperature were recorded using a fluorescence spectrophotometer (F-4600, Hitachi, Japan). A 150 W Xe lamp was selected as the excitation source, and the photomultiplier tube was working at 500 V. The CIE chromaticity coordinates were calculated according to the spectrum data. The schematic energy level diagram for the excitation and emission process of $Er^{3+}$ and $Sm^{3+}$ in LMA was calculated based on the electronic energy levels in the trivalent lanthanide aquo ions [31]. The decay curves were recorded using a spectrofluorometer (FLS 980, Edinburgh Instruments Ltd., UK) using a 250 nm pulse laser as the excitation source. The temperature-dependent decay curves were recorded on the same spectrofluorometer with an automatic temperature-controlled heating holder. The temperature-dependent PL spectra were measured on the spectrophotometer (F-4600, Hitachi, Japan), combined with a self-made heating attachment and a computer-controlled electric furnace. Quantum yields were measured on a fluoromax-4 spectrofluorometer (Horiba Jobin Yvon, France) with an integral sphere at room temperature.

**2.3 Calculation for the decay lifetimes**

Based on the decay curves, the lifetimes of the LMA: $Er^{3+}$, $Sm^{3+}$ phosphors are calculated according to the following equation [32]:

$$I = I_0 exp(-t/\tau) \quad (1)$$

where $\tau$ is the lifetime, $I_0$ and $I$ are the emission intensity at the initial time and time $t$, respectively. The temperature-dependent decay curves of the LMA: $Er^{3+}$ and LMA: $Er^{3+}$, $Sm^{3+}$ phosphors are measured in a special heating holder at the same excitation and monitoring wavelength. And the PL lifetimes were also calculated according to Eq. (1).

**2.4 Calculation for the interaction of energy transfer**

The multipolar interaction of energy transfer between $Er^{3+}$ and $Sm^{3+}$ ions, Dexter's energy transfer expressions of multipolar interaction and Reisfeld's approximation are simplified as follows [33]:

$$I_0/I_y \propto C^{n/3} \quad (2)$$

where $I_0$ and $I_y$ are the luminescence intensity of LMA: $0.01Er^{3+}/ ySm^{3+}$ phosphors with the absence and presence of $Sm^{3+}$, and $C$ is the sum of the doping concentration of $Er^{3+}$ and $Sm^{3+}$ ions. The value $n$ stands for the multipolar interaction of energy transfer, for which $n$= 6, 8, 10 represent the dipole-dipole (d-d), dipole-quadrupole (d-q), and quadrupole-quadrupole (q-q) interactions, respectively.

**2.5 Quantum yield, correlated color temperature and color rendering index**

In addition, important factors for practical wLEDs of phosphors, the quantum yield (QY), correlated color temperature (CCT) and color rendering index (Ra) were also studied. Herein, the quantum yields of LMA: $0.1Er^{3+}$, $ySm^{3+}$ phosphors were measured

under the excitation at 255 nm. The recorded QYs of LMA: 0.1$Er^{3+}$, $y$$Sm^{3+}$ phosphors (y=0, 0.01, 0.03, 0.05, 0.08, and 0.1) are 0.31, 0.30, 0.36, 0.38, 0.39, and 0.23, respectively. The CCT and Ra of LMA: 0.1$Er^{3+}$, 0.01$Sm^{3+}$ phosphor were calculated to be 7096 and 85, under the excitation at 254 nm.

## 3. Results and Discussion

### 3.1 Phase, crystal structure, and morphology

The XRD patterns of the LMA phosphors and LMA doped with various rare-earth ions (LMA: $Er^{3+}$, LMA: $Sm^{3+}$, and LMA: $Er^{3+}$, $Sm^{3+}$) are illustrated in Fig. S1. All peaks can be indexed to LMA (No. 78-1845). The lack of trace peaks in Fig. S1 indicates that the phosphor is pure single-phase LMA, and the sharpness of the peaks shows that the crystallinity is good. The Rietveld refinement shows that the $Er^{3+}$ and $Sm^{3+}$ are doped on the $La^{3+}$ site (Fig. 2a, Table S1). The crystal lattice structure of LMA: 0.1$Er^{3+}$, 0.08$Sm^{3+}$ based on the refinement results is made up of two lattice units (Fig. 2b), in which $La^{3+}$ (or $Er^{3+}$/ $Sm^{3+}$) coordinate with twelve oxygen ions in the $LaO_{12}$ (or $ErO_{12}$ or $SmO_{12}$) coordination polyhedron. All the LMA: 0.1$Er^{3+}$, LMA: 0.08$Sm^{3+}$, and LMA: 0.1$Er^{3+}$, 0.08$Sm^{3+}$ phosphors have a platelet morphology with a thickness of around 0.5 μm and lateral size of 2-5 μm (Figs. 2c-e, Fig. S2); a size optimal for phosphor luminous efficiency and wLED encapsulation. The EDS mapping indicates that Er and Sm elements are evenly distributed in the platelets (Fig. S2) with an atomic ratio of 7:1, agreeing with the target stoichiometric composition (Fig. 2f).

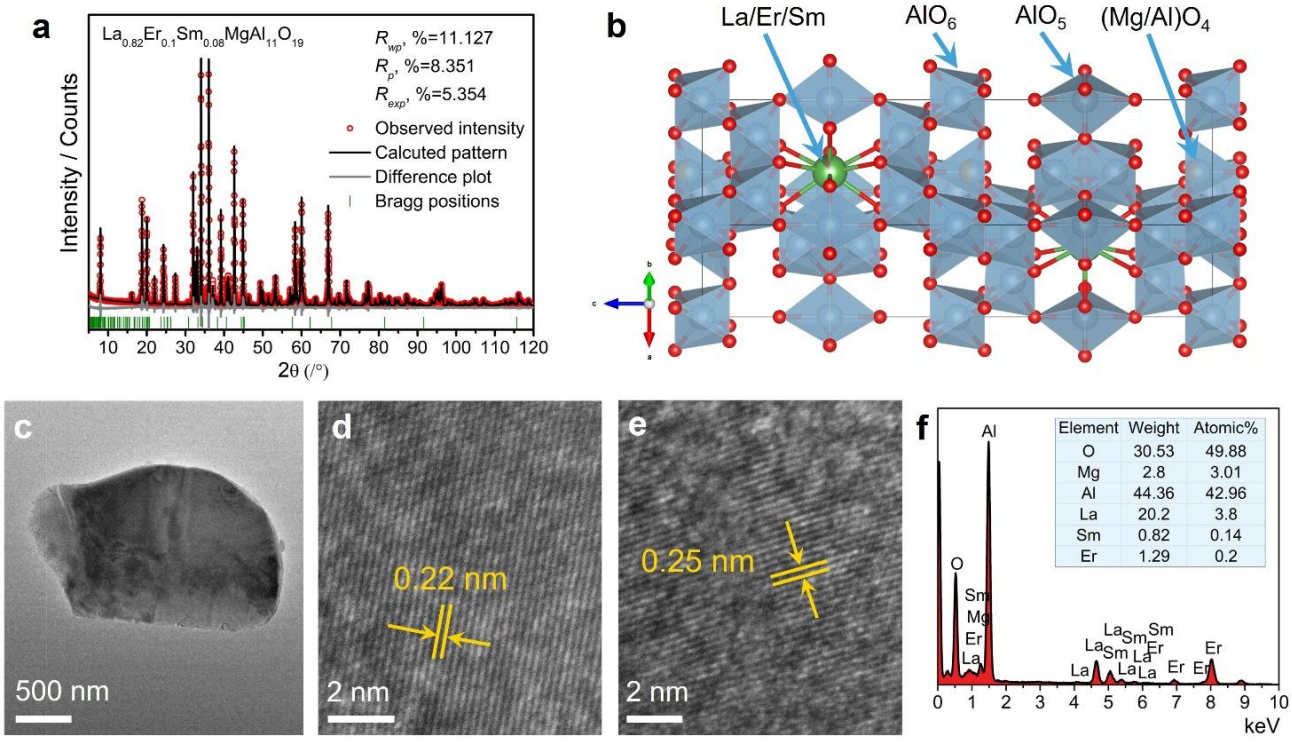


**Fig. 2. Phase, crystal structure, and morphology of the LMA: 0.1$Er^{3+}$, 0.08$Sm^{3+}$ phosphor.** (a) Rietveld refinement of the X-ray diffraction data indicating the co-doped sample hexagonal packed crystal structure with the space group of P63/mmc. (b) Crystal lattice structure showing sites of $La^{3+}$ are occupied by $La^{3+}$, $Er^{3+}$ and $Sm^{3+}$ ions with the occupation proportion p=0.890,

0.074 and 0.036, respectively. The cell parameters of the as-prepared LMA: 0.1$Er^{3+}$, 0.08$Sm^{3+}$ product are a=b= 5.59Å, c= 21.95Å, and the cell volume at 594.07$Å^3$ is smaller than those of pristine LMA structure. (c) TEM and (d, e) HRTEM images of the LMA: 0.1$Er^{3+}$, 0.08$Sm^{3+}$ phosphor showing that the d-pacing of (204) and (114) planes of LMA with 0.22 and 0.25 nm, respectively. (f) The EDS spectrum recorded in (c) with an inset table showing the detailed data of the EDS spectrum including elements of La, Mg, Al, O, Sm, and Er.

### 3.2 Luminescence properties of LMA: *x*$Er^{3+}$

The LMA: x$Er^{3+}$ phosphors excited by a 255 nm UV light (Fig. 3a left) generate one of the corresponding emission peaks at 402 nm (Fig. 3a right) that LMA: $Sm^{3+}$ could absorb. When LMA: $Sm^{3+}$ absorbs light at 403 nm it emits 594 nm light (orange-reddish) (Fig. 3b). The most substantial absorption peak of LMA: $Sm^{3+}$ closely overlaps with the strongest emission peak of LMA: x$Er^{3+}$ (Fig. S3). This indicates multi-channel relaxation pathways during energy transfer from $Er^{3+}$ to $Sm^{3+}$ and results in white light. The concentration quenching occurred at *x*=0.1, suggesting that 255 nm is a more suitable excitation source than the normal source at 378 nm because of the efficient variable radiative probability of $Er^{3+}$ (Fig. 3c, Figs. S4-5).

### 3.3 Energy transfer behavior of LMA: $Er^{3+}$, $Sm^{3+}$ phosphors

To prove the energy transfer between $Er^{3+}$ and $Sm^{3+}$, the emission spectra of LMA: 0.1$Er^{3+}$, *y*$Sm^{3+}$ with different $Sm^{3+}$ concentrations are recorded and shown in Fig. 3d. The spectra split between the emissions of $Er^{3+}$ (350 to 550 nm) and $Sm^{3+}$ (550 to 700 nm). With increasing $Sm^{3+}$ concentration, the emission intensity of $Er^{3+}$ significantly decreases, and the emission intensity of $Sm^{3+}$ increases (Fig. 3e), further proving that the energy transfer from $Er^{3+}$ to $Sm^{3+}$ within the LMA host. The maximum $Sm^{3+}$ emission intensity is observed at y=0.08 before concentration quenching.

To further investigate the energy transfer from $Er^{3+}$ to $Sm^{3+}$, the PL decay curves of LMA: $Er^{3+}$, $Sm^{3+}$ in Fig. 3f are measured, which decrease gradually with the increasing concentration of $Sm^{3+}$ ions. As shown in Table S2, the lifetimes of $Er^{3+}$ ions in LMA: $Er^{3+}$, $Sm^{3+}$ phosphors are calculated to be 270.0, 267.4, 184.2, 166.9, and 146.6 μs, which decrease with increasing $Sm^{3+}$ concentration. The energy transfer from $Er^{3+}$ to $Sm^{3+}$ finds another evidence from the decrease in lifetimes of LMA: $Er^{3+}$, $Sm^{3+}$ phosphors with increasing $Sm^{3+}$ concentrations, as indicated by the PL decay curves in Fig. 3f (Fig. S6 and Table S2). When the LMA: $Er^{3+}$, $Sm^{3+}$ phosphors are excited at 260 nm, the energy of $Er^{3+}$ electrons at a high energy state are transferred to $Sm^{3+}$ by energy level resonance and photon energy reabsorption. The electrons of $Sm^{3+}$ are then effectively excited from the valence band to the conduction band, finally resulting in the emission of $Sm^{3+}$ when the electrons relax back to the valence band (Fig. 5a).

The following equation calculates the energy transfer efficiency ($\eta_{et}$):

$$\eta_{et} = 1 - \tau_y/\tau_0 \quad (3)$$

where $\tau_y$ and $\tau_0$ are the lifetimes of $Er^{3+}$ with and without the co-doped $Sm^{3+}$, respectively. The $\eta_{et}$ increases with the increase of the $Sm^{3+}$ content, as shown in Table S2, further confirming the energy transfer process. The multipolar interaction of energy

transfer between $Er^{3+}$ and $Sm^{3+}$ is analyzed by a simplified Dexter's energy transfer expressions of multipolar interaction and Reisfeld's approximation [34]. According to the value of $R^2$ (Fig. S7), in the best linear relationship, when $n$= 10, the mechanism that governs the energy transfer from $Er^{3+}$ to $Sm^{3+}$ in the LMA host is quadrupole-quadrupole interaction.

Manipulation of the emission feature of LMA: $Er^{3+}$, $Sm^{3+}$ allows us to tune its PL spectra and emission color from blue to white and then to the red region with increasing $Sm^{3+}$ concentration as confirmed by the calculated CIE coordinates (Fig. S8, Table S3). The CIE coordinate of LMA: $0.1Er^{3+}$, $0.01Sm^{3+}$ at (0.3141, 0.2791) is close to white light. In addition, QY and CCT of LMA: $0.1Er^{3+}$, 0.01 $Sm^{3+}$ phosphors are 0.30 and 7096, respectively, under the same excitation light. When fabricated into an LMA: $0.1Er^{3+}$, $0.01Sm^{3+}$-based wLED with a deep-UV LED chip (λ=254 nm) (Fig. S9), it can also exhibit bright white emission stable with a stable color coordinate (0.3012, 0.2913) and high color rendering index (Ra) (92.5). The more appropriate CIE, CCT and higher Ra value than the commercial YAG: $Ce^{3+}$ wLEDs demonstrate that the LMA: $Er^{3+}$, $Sm^{3+}$ is a promising candidate for single-phase white-emitting phosphor for commercial wLEDs (Table S4).

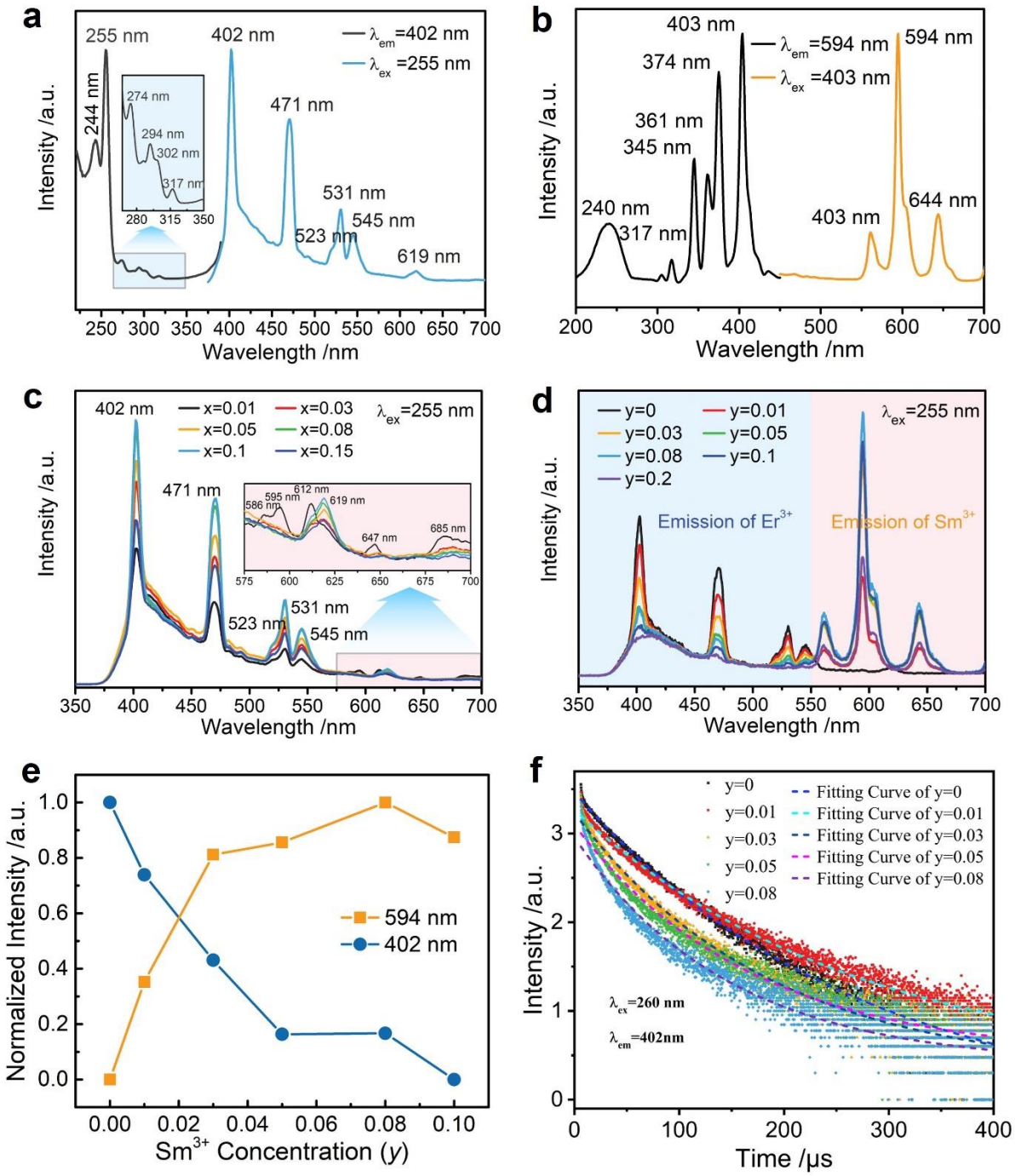


**Fig. 3. Luminescence properties of the LMA: $Er^{3+}$/ $Sm^{3+}$ phosphor.** (a) PLE ($\lambda_{em}$=402 nm) and PL ($\lambda_{ex}$=255 nm) spectra of LMA: 0.1$Er^{3+}$. The emission peaks centered at 402, 471, 523, 531, 545, and 619 nm specifically correspond to the $^4P_{3/2}\rightarrow{}^4I_{13/2}$, $^4P_{3/2}\rightarrow{}^4I_{11/2}$, $^2H_{11/2}\rightarrow{}^4I_{15/2}$, $^4P_{3/2}\rightarrow{}^4I_{9/2}$, $^4S_{3/2}\rightarrow{}^4I_{15/2}$, and $^4P_{3/2}\rightarrow{}^4F_{9/2}$ transition from the energy data for different energy levels of $Er^{3+}$. The inset presents the magnified PLE spectrum. (b) The PLE ($\lambda_{em}$=594 nm) and PL ($\lambda_{ex}$=403 nm) spectra of LMA: 0.08$Sm^{3+}$ sample. The emission peaks at 561, 594, and 644 nm originate from the $^4G_{5/2}\rightarrow{}^6H_J$ (J= 5/2, 7/2, 9/2) transitions. (c) PL spectra of LMA: *x*$Er^{3+}$ phosphors with different $Er^{3+}$ concentration. The inset shows some weak emission peaks in the long-wavelength regions. (d) PL spectra of LMA: 0.1$Er^{3+}$, *y*$Sm^{3+}$ phosphors (*y*= 0, 0.01, 0.03, 0.05, 0.08, 0.1, 0.2), and (e) the dependence of the

emission intensity of the peaks at 402 nm and 594 nm on $Sm^{3+}$ doping concentration. (f) PL decay curves of $Er^{3+}$ in LMA: $0.1Er^{3+}$, $ySm^{3+}$ phosphors excited at 260 nm and monitored at 402 nm.

### 3.4 Negative-thermal-quenching behavior for practical application

The thermal performance of LMA: $0.1Er^{3+}$, $0.01Sm^{3+}$ phosphor as a white light source was examined. It shows "negative-thermal-quenching" behavior, where the emission intensity increases with increasing the temperature (Figs. 4a, b). As shown in Fig. 4b, the emission intensity of $Er^{3+}$ rises to 323 K and then slowly decreases at higher temperatures. On the other hand, the intensity of $Sm^{3+}$ increases continuously with temperature from 298 K to 573 K. As a result, the combined emission intensities showed a steady-state increase with a value at 423 K, approximately 125% of that at room temperature (298 K). Furthermore, the constant CIE coordinates at different temperatures (Fig. S10, Table S5) indicate stable color rendering at high temperatures (up to 573 K). Similar intensity trends were also observed in the temperature-dependent PL spectra of LMA: $0.1Er^{3+}$, $0.03Sm^{3+}$ phosphors (Fig. S11).

The integrated PL intensity ratio (P) of $Er^{3+}$ to $Sm^{3+}$ emission is used as a thermometric parameter [35, 36]. When P ratios are normalized with respect to room temperature value, the normalized intensity ratio ($P/P_{273\ K}$) correlates linearly with the temperatures (T) over a very wide range from 298 to 523 K (Fig. 4c), which is described in the equation below:

$$T = 844.0 - 571.4\frac{P}{P_{273\ K}} \quad (4)$$

The more accurate linear correlation between the natural logarithm of ratio (*lnP*) and the inverse of temperature is obtained to confirm its sensitivity (Fig. 4d) further. The relative sensitivity ($S_r$) is further calculated based on the following equation (5)[37]:

$$S_r = \frac{\delta P/\delta T}{P} \quad (5)$$

The inset indicates that the maximum $S_r$ is as high as 0.33% $K^{-1}$ at 573 K (Figs. S12 and S13), which confirms extraordinary sensitivity and wider sensing range than the previously reported thermal range in optical thermometry (Table S6) [38]. Furthermore, the relationship between natural logarithm of ratio (*lnP*) *vs.* the inverse of temperature can also be used as an alternative to gain a more accurate linear correlation (Fig. 4d). The temperature dependence of *lnP* follows the equation:

$$\ln P = \frac{409.6}{T} - 0.5 \quad (6)$$

This corresponding goodness of the plot ($R^2$=0.9896) is much higher than that in Fig. 4c. And the slope of 571.4 and 409.6 are also several times larger than that in previous studies. Therefore, the LMA: $Er^{3+}$, $Sm^{3+}$ phosphor can also be considered as a candidate for UV-excited luminescent ratiometric thermometer with high sensitivity and wide temperature-sensing range.

## 4. Discussion

The temperature enhancing performance of the LMA: $Er^{3+}$, $Sm^{3+}$ phosphors can be attributed to several factors. The outstanding thermal stability of LMA: $Er^{3+}$, $Sm^{3+}$ phosphors is inherited from the LMA host due to its complicated dense networked

magnetoplumbite-type structure [39, 40]. Defects formed during materials synthesis may trap thermally reactivated electrons to compensate for TQ, as indicated by the initial increase in emission intensity of $Er^{3+}$ (Fig. 4b). At room temperature, the activator absorbs part of the energy to produce UC emission, and the remaining electrons are captured by nearby defects. As the temperature gradually increases, the electrons in the defect state are released into the excited state around the activator by thermal activation, inducing the excited state to release more electrons, lead to the enhancement of UC emission[41-43]. The energy transfer behavior through photon cascade excitation from $Er^{3+}$ to $Sm^{3+}$ is the key to the negative-thermal-quenching behavior. The continuous increase of $Sm^{3+}$ emission at the expense of $Er^{3+}$ emission leads to the overall improvement in intensity with temperature. The intensity enhancement indicates the nonradiative transition of $Er^{3+}$ is mitigated by the enhanced energy transfer from $Er^{3+}$ to $Sm^{3+}$. The temperature-dependent PL decay curves in Fig. 4e and Fig. S14 indicate the PL lifetimes of the LMA: $Er^{3+}$, $Sm^{3+}$ are calculated to be 190.1, 178.7, 173.6, 154.6, and 136.4 μs at 298, 348, 398, 448, and 498 K, respectively, which further confirm that the lifetimes of $Eu^{3+}$ ions decrease as the temperature rises. The energy transfer efficiency from $Er^{3+}$ to $Sm^{3+}$ at 498 K, calculating based on Eq. (3), improves by five times compared to that at room temperature (Table S7), which is reflected by the more extensive overlap between the $Er^{3+}$ emission and $Sm^{3+}$ excitation with higher temperature. The broadening of the full width at half-maximum of the peaks due to amplitude increment by stronger ionic vibration of $Er^{3+}$ and $Sm^{3+}$ at high temperature is the main reason for more extensive overlap. These processes establish highly efficient negative-thermal-quenching behavior in LMA: $Er^{3+}$, $Sm^{3+}$ phosphors.

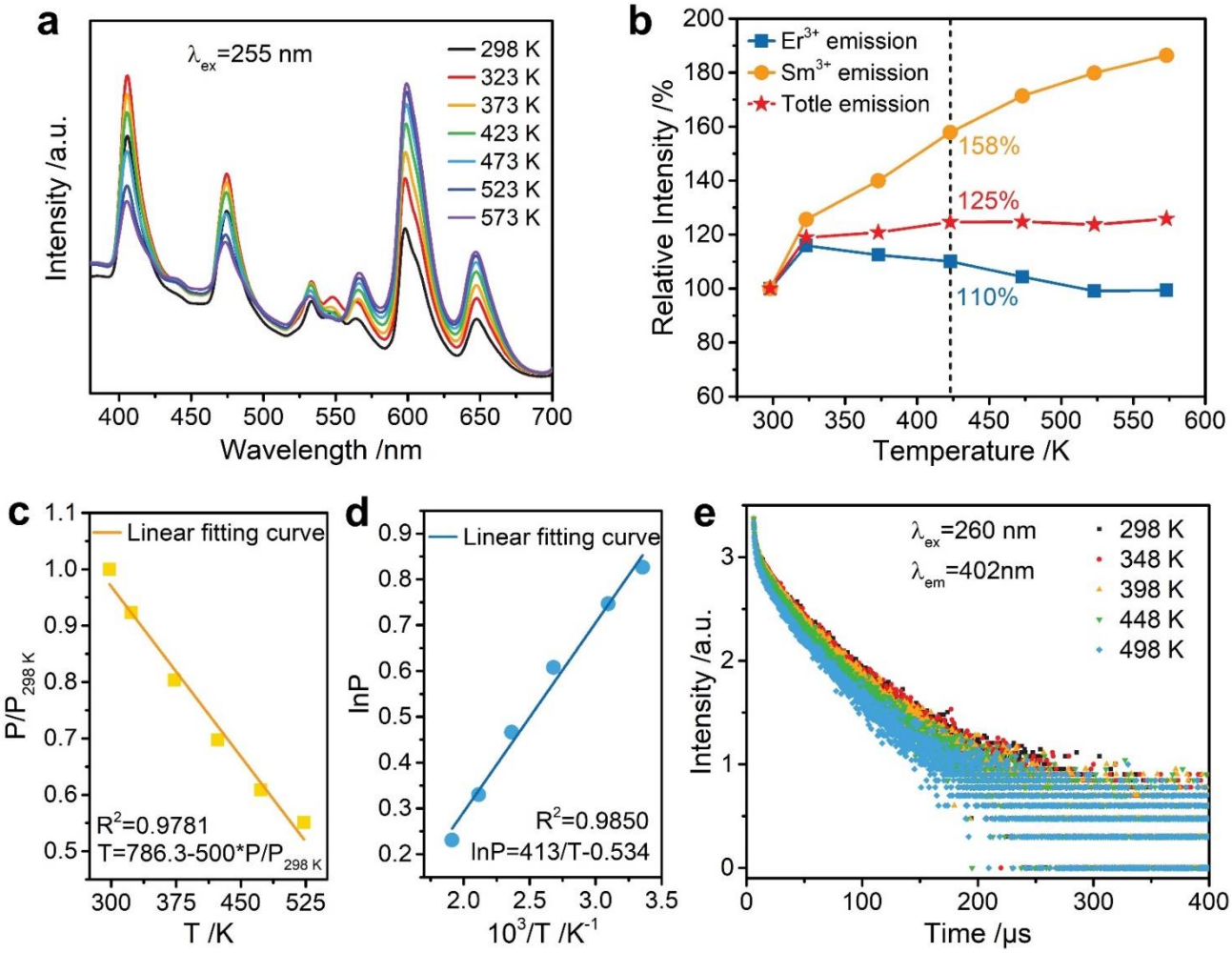


**Fig. 4. Negative-thermal-quenching behavior of the LMA: $Er^{3+}$, $Sm^{3+}$ phosphor.** (a) Temperature-dependent emission spectra of LMA: $0.1Er^{3+}$, $0.01Sm^{3+}$ phosphor under 255 nm excitation in the temperature range 298-573 K. (b) Temperature-dependent integrated emission intensity of $Er^{3+}$ (ranging from 380 to 550 nm) and $Sm^{3+}$ (ranging from 550 to 700 nm) in LMA: $0.1Er^{3+}$, $0.01Sm^{3+}$ from 298 K to 573 K. (c) Temperature-dependent thermometric parameter ($P/P_{298\ K}$) of LMA: $0.1Er^{3+}$, $0.01Sm^{3+}$ phosphor. P is equal to the ratio of $I_{Er}/I_{Sm}$, where $I_{Er}$ and $I_{Sm}$ are the integrated intensity in the range of 380-550 and 550-700 nm, respectively. (d) The natural logarithm of ratio P (lnP) changing with the inverse of temperature. (e) Temperature-dependent PL decay curves of $Er^{3+}$ ions in LMA: $0.1Er^{3+}$, $0.01Sm^{3+}$ phosphor.

Thus, the energy transfer process is proposed and depicted in Fig. 5a. When the LMA: $Er^{3+}$, $Sm^{3+}$ phosphors are excited at 255 nm, electrons in the $^4I_{15/2}$ level of $Er^{3+}$ ions could absorb the photon energy and are firstly excited to the $^4D_{7/2}$ level, then randomly relax to the $^4P_{3/2}$, $^2H_{11/2}$ and $^4S_{3/2}$ level by non-radiative relaxation, further relax to lower energy level and result in the emission features of $Er^{3+}$ ions. Meanwhile, the energy released from high energy state $^4P_{3/2}$ band to low energy state $^4I_{13/2}$ band by $Er^{3+}$ ions also transfer to $Sm^{3+}$ ions by energy level resonance and photon energy reabsorption, then effectively excite the electrons of $Sm^{3+}$ ions from valence band ($^6H_{5/2}$) to conduction band ($^4F_{2/7}$), and finally obtain the emission of $Sm^{3+}$ ions when the electrons relax

back to the valence band. This indicated that there are multi-channel relaxation pathways during energy transfer process (Fig.S3). The simplified configurational coordinate diagram in Fig. 5b explains the tendency of the $Er^{3+}$ to $Sm^{3+}$ emission with increasing temperatures. Under the excitation at UV light, the electrons of $Er^{3+}$ are excited from the ground state ($^4I_{15/2}$) to the excited state ($^4P_{3/2}$, $^4S_{3/2}$, $^2H_{11/2}$), then relax to the bottom of the conduction band (point B and C). As a result, blue and green emission lights are emitted before returning to the ground state. At higher temperatures, more energy is available to overcome the energy barriers ($\Delta E_1$ and $\Delta E_2$) and move the electrons from B (or C) to D (or E) and then return to the ground state through nonradiative relaxation, resulting in the thermal quenching in the absence of $Sm^{3+}$. Since the energy barrier ($\Delta E_1$ and $\Delta E_2$) is relatively high for the phosphor doped only with $Er^{3+}$, the emission of $Er^{3+}$ shows excellent thermal stability. For the $Er^{3+}$ and $Sm^{3+}$ co-doped samples, an energy threshold $\Delta E_3$ for energy transfer from $Er^{3+}$ to $Sm^{3+}$ is obtained, possibly lower than $\Delta E_1$. As the temperature increases, more excited electrons can overcome the energy barrier $\Delta E_3$ through electron-phonon coupling and improve the energy transfer efficiency from $Er^{3+}$ to $Sm^{3+}$ reflected as movement from point F to G. In addition, the energy barrier $\Delta E_4$ for the thermal activation of $Sm^{3+}$ is also large. Hence, the most excited electrons would go back to the ground state through a $^4G_{5/2} \rightarrow {}^6H_J$ allowed transition without thermal quenching, thus explaining the negative-thermal-quenching effect[44, 45]. Therefore, apart from the defect-trap theory, the energy transfer process for electron migration also plays an essential role in improving the thermal property of phosphors, which can be further applied to other thermally stable phosphors (Fig. S15).

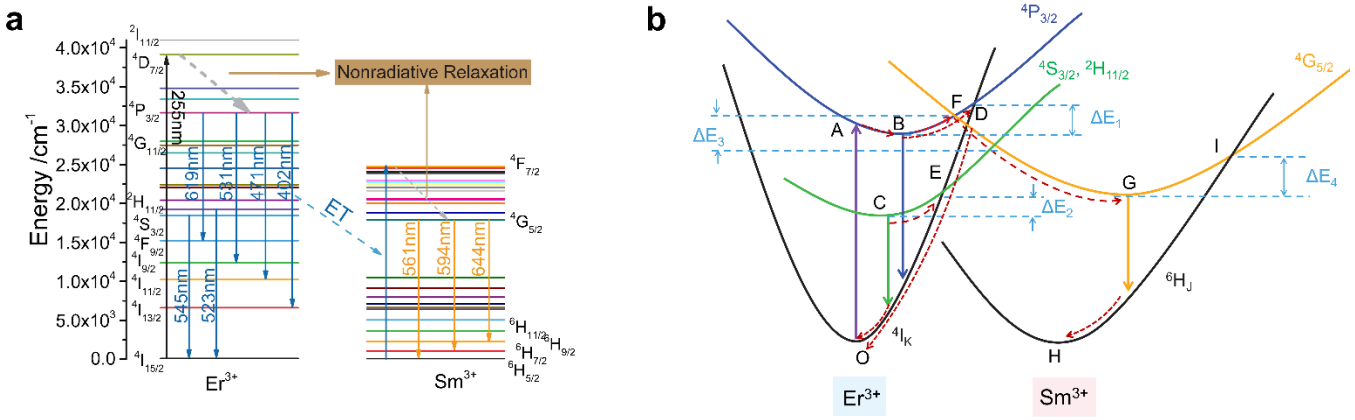


**Fig. 5. The mechanism for the negative-thermal-quenching behavior.** (a) Schematic energy level diagram for the excitation and emission process of $Er^{3+}$ and $Sm^{3+}$ in LMA host. When excited at 255 nm, electrons in the $^4I_{15/2}$ level of $Er^{3+}$ absorb the photon energy and are excited to the $^4D_{7/2}$ level then randomly relax to the $^4P_{3/2}$, $^2H_{11/2}$ and $^4S_{3/2}$ level by nonradiative relaxation and further relax to lower energy level and result in the unique blue emission features of $Er^{3+}$. (b) The simplified configurational coordinate diagram of the ground and excited states of $Er^{3+}$ and $Sm^{3+}$.

## 5. Conclusion

In conclusion, we introduced a negative-thermal-quenching phosphor LMA: $Er^{3+}$, $Sm^{3+}$ with outstanding thermal stability and enhanced emission intensity. When excited by 255 nm light, an obvious overlap between the emission peak of $Er^{3+}$ and the excitation peak of $Sm^{3+}$ in LMA is formed. This effectively prompted a thermally enhanced energy transfer process from $Er^{3+}$ to $Sm^{3+}$ to improve the emission intensity of $LaMgAl_{11}O_{19}$: $Er^{3+}$, $Sm^{3+}$ phosphors up to 573 K. The favorable thermal stability and preferable CIE coordinates indicates that LMA: $Er^{3+}$, $Sm^{3+}$ is expected to be a candidate material for wLEDs. Our work provides a design concept for future light conversion materials with negative-thermal-quenching properties. These materials can be used for various applications, including but not limited to high power wLED operations and high temperature radiometric optical thermometry with great sensitivity and wide-temperature-sensing range.

## Credit author statement

Xin Min: Conceptualization, Methodology, Writing - Original Draft. Cheng-Yen Lao and Amr. M. Abdelkader: Software, Validation. Yifei Liu: Writing - Review & Editing. Haipeng Ji and Xiaowen Wu: Visualization, Data Curation. Yan'gai Liu, Zhaohui Huang and Minghao Fang: Resources, Supervision, Project administration. Ramachandran Vasant Kumar and Kai Xi: Conceptualization, Supervision, Formal analysis.

## Declaration of Competing Interest

The authors declare that they have no known competing financial interests or personal relationships that could have appeared to influence the work reported in this paper.


## Acknowledgements

This work was financially supported by the National Natural Science Foundation of China (No. 52174379), the Young Elite Scientist Sponsorship Program by CAST (YESS20200103), and the Fundamental Research Funds for the Central Universities (No. 265QZ2022004). H. Ji thanks the Postdoctoral Research Sponsorship in Henan Province under Grant No. 19030025.

## REFERENCES


[1] P.F. Smet, J.J. Joos, Stabilizing colour and intensity, Nature Materials 16(5) (2017) 500-501. https://doi.org/10.1038/nmat4901.

[2] M. Li, Z. Xia, Recent progress of zero-dimensional luminescent metal halides, Chemical Society Reviews 50(4) (2021) 2626-2662. https://doi.org/10.1039/D0CS00779J.

[3] H. Liao, M. Zhao, M.S. Molokeev, Q. Liu, Z. Xia, Learning from a Mineral Structure toward an Ultra-Narrow-Band Blue-Emitting Silicate Phosphor RbNa3(Li3SiO4)4:Eu2+, Angewandte Chemie International Edition 57(36) (2018) 11728-11731. https://doi.org/https://doi.org/10.1002/anie.201807087.

[4] M. Zhao, Z. Xia, X. Huang, L. Ning, R. Gautier, M.S. Molokeev, Y. Zhou, Y.-C. Chuang, Q. Zhang, Q. Liu, K.R. Poeppelmeier, Li substituent tuning of LED phosphors with enhanced efficiency, tunable photoluminescence, and improved thermal stability, Science Advances 5(1) (2019) eaav0363. https://doi.org/doi:10.1126/sciadv.aav0363.

[5] C.-H. Huang, T.-M. Chen, A Novel Single-Composition Trichromatic White-Light Ca3Y(GaO)3(BO3)4:Ce3+,Mn2+,Tb3+ Phosphor for UV-Light Emitting Diodes, The Journal of Physical Chemistry C 115(5) (2011) 2349-2355. https://doi.org/10.1021/jp107856d.

[6] C.-K. Chang, T.-M. Chen, Sr3B2O6:Ce3+,Eu2+: A potential single-phased white-emitting borate phosphor for ultraviolet light-emitting diodes, Applied Physics Letters 91(8) (2007) 081902. https://doi.org/10.1063/1.2772195.

[7] G. Zhou, B. Su, J. Huang, Q. Zhang, Z. Xia, Broad-band emission in metal halide perovskites: Mechanism, materials, and applications, Materials Science and Engineering: R: Reports 141 (2020) 100548. https://doi.org/https://doi.org/10.1016/j.mser.2020.100548.

[8] G.H. Muñoz, C.L. de la Cruz, A.F. Muñoz, J.O. Rubio, High-temperature luminescence properties of Eu2+-activated alkali halide phosphor materials, Journal of Materials Science Letters 7(12) (1988) 1310-1312. https://doi.org/10.1007/BF00719967.

[9] P. Dorenbos, Thermal quenching of Eu2+ 5d–4f luminescence in inorganic compounds, Journal of Physics: Condensed Matter 17(50) (2005) 8103. https://doi.org/10.1088/0953-8984/17/50/027.

[10] J. Qiao, L. Ning, M.S. Molokeev, Y.-C. Chuang, Q. Liu, Z. Xia, Eu2+ Site Preferences in the Mixed Cation K2BaCa(PO4)2 and Thermally Stable Luminescence, Journal of the American Chemical Society 140(30) (2018) 9730-9736. https://doi.org/10.1021/jacs.8b06021.

[11] L. Wang, W. Li, L. Yin, Y. Liu, H. Guo, J. Lai, Y. Han, G. Li, M. Li, J. Zhang, R. Vajtai, P.M. Ajayan, M. Wu, Full-color fluorescent carbon quantum dots, Science Advances 6(40) (2020) eabb6772. https://doi.org/doi:10.1126/sciadv.abb6772.

[12] Q. Wei, J. Ding, Y. Wang, A novel tunable extra-broad yellow-emitting nitride phosphor with zero-thermal-quenching property, Chemical Engineering Journal 386 (2020) 124004. https://doi.org/https://doi.org/10.1016/j.cej.2019.124004.

[13] Y. Zhuo, A. Mansouri Tehrani, A.O. Oliynyk, A.C. Duke, J. Brgoch, Identifying an efficient, thermally robust inorganic phosphor host via machine learning, Nature Communications 9(1) (2018) 4377. https://doi.org/10.1038/s41467-018-06625-z.

[14] W.B. Im, N. George, J. Kurzman, S. Brinkley, A. Mikhailovsky, J. Hu, B.F. Chmelka, S.P. DenBaars, R. Seshadri, Efficient and Color-Tunable Oxyfluoride Solid Solution Phosphors for Solid-State White Lighting, Advanced Materials 23(20) (2011) 2300-2305. https://doi.org/https://doi.org/10.1002/adma.201003640.

[15] C.C. Lin, R.-S. Liu, Advances in Phosphors for Light-emitting Diodes, The Journal of Physical Chemistry Letters 2(11) (2011) 1268-1277. https://doi.org/10.1021/jz2002452.

[16] T. Takeda, N. Hirosaki, S. Funahshi, R.-J. Xie, Narrow-Band Green-Emitting Phosphor Ba2LiSi7AlN12:Eu2+ with High Thermal Stability Discovered by a Single Particle Diagnosis Approach, Chemistry of Materials 27(17) (2015) 5892-5898. https://doi.org/10.1021/acs.chemmater.5b01464.

[17] G.-H. Pan, H. Wu, S. He, L. Zhang, Z. Hao, X. Zhang, J. Zhang, Dye-embedded YAG:Ce3+@SiO2 composite phosphors toward warm wLEDs through radiative energy transfer: preparation, characterization and luminescence properties, Nanoscale 10(47) (2018) 22237-22251. https://doi.org/10.1039/C8NR07360K.

[18] G. Blasse, Thermal Quenching of Characteristic Fluorescence, The Journal of Chemical Physics 51(8) (1969) 3529-3530. https://doi.org/10.1063/1.1672543.

[19] C.C. Lin, Y.-T. Tsai, H.E. Johnston, M.-H. Fang, F. Yu, W. Zhou, P. Whitfield, Y. Li, J. Wang, R.-S. Liu, J.P. Attfield, Enhanced Photoluminescence Emission and Thermal Stability from Introduced Cation Disorder in Phosphors, Journal of the American Chemical Society 139(34) (2017) 11766-11770. https://doi.org/10.1021/jacs.7b04338.

[20] Y. Wei, H. Yang, Z. Gao, Y. Liu, G. Xing, P. Dang, A.A.A. Kheraif, G. Li, J. Lin, R.-S. Liu, Strategies for Designing Antithermal-Quenching Red Phosphors, Advanced Science 7(8) (2020) 1903060. https://doi.org/https://doi.org/10.1002/advs.201903060.

[21] S. Liu, X. Fang, B. Lu, D. Yan, Wide range zero-thermal-quenching ultralong phosphorescence from zero-dimensional metal halide hybrids, Nature Communications 11(1) (2020) 4649. https://doi.org/10.1038/s41467-020-18482-w.
[22] H. Zhang, Y. Su, J. Zhang, Z. Ni, X. Zhang, Controllable structural ordering via chemical substitution to the efficient and thermally stable luminescence in NASICON-type phosphor Series: Na1+xHf2−xScx(PO4)3:Eu, Chemical Engineering Journal 426 (2021) 130778. https://doi.org/https://doi.org/10.1016/j.cej.2021.130778.
[23] Y. Wei, H. Yang, Z. Gao, X. Yun, G. Xing, C. Zhou, G. Li, Anti-Thermal-Quenching Bi3+ Luminescence in a Cyan-Emitting Ba2ZnGe2O7:Bi Phosphor Based on Zinc Vacancy, Laser & Photonics Reviews 15(1) (2020). https://doi.org/10.1002/lpor.202000048.
[24] L. Wu, Y. Bai, L. Wu, H. Yi, Y. Kong, Y. Zhang, J. Xu, Sm3+ and Eu3+ codoped SrBi2B2O7: a red-emitting phosphor with improved thermal stability, RSC Advances 7(2) (2017) 1146-1153. https://doi.org/10.1039/c6ra26752a.
[25] R.R. Wang, G.H. Li, G.M. Cai, Thermal-stability synergy improvement of Sm<SUP>3+</SUP> and Eu<SUP>3+</SUP> in Ca<sub>3.6</sub>In<sub>3.6</sub>(PO<sub>4</sub>)<sub>6</sub>: the effect of local symmetry, JOURNAL OF MATERIALS CHEMISTRY C 11(10) (2023) 3616-3625. https://doi.org/10.1039/d2tc05406j.
[26] Y.H. Kim, P. Arunkumar, B.Y. Kim, S. Unithrattil, E. Kim, S.-H. Moon, J.Y. Hyun, K.H. Kim, D. Lee, J.-S. Lee, W.B. Im, A zero-thermal-quenching phosphor, Nature Materials 16(5) (2017) 543-550. https://doi.org/10.1038/nmat4843.
[27] J. Zhong, Y. Zhuo, S. Hariyani, W. Zhao, W. Zhuang, J. Brgoch, Thermally Robust and Color-Tunable Blue-Green-Emitting BaMgSi4O10:Eu2+,Mn2+ Phosphor for Warm-White LEDs, Inorganic Chemistry 59(18) (2020) 13427-13434. https://doi.org/10.1021/acs.inorgchem.0c01803.
[28] R. Wei, L. Yang, X. Zhang, X. Tian, X. Peng, F. Hu, H. Guo, Energy transfer and highly thermal stability in single-phase SrY2O4:Bi3+,Sm3+ phosphors for UV-LEDs, Journal of Luminescence 228 (2020) 117606. https://doi.org/https://doi.org/10.1016/j.jlumin.2020.117606.
[29] G.B. Nair, H.C. Swart, S.J. Dhoble, A review on the advancements in phosphor-converted light emitting diodes (pc-LEDs): Phosphor synthesis, device fabrication and characterization, Progress in Materials Science 109 (2020) 100622. https://doi.org/https://doi.org/10.1016/j.pmatsci.2019.100622.
[30] L. Haoran, W. Chang-An, Z. Chenguang, T. Shuyan, Thermo-physical properties of rare-earth hexaaluminates LnMgAl11O19 (Ln: La, Pr, Nd, Sm, Eu and Gd) magnetoplumbite for advanced thermal barrier coatings, Journal of the European Ceramic Society 35(4) (2015) 1297-1306. https://doi.org/https://doi.org/10.1016/j.jeurceramsoc.2014.10.030.
[31] W.T. Carnall, P.R. Fields, K. Rajnak, Electronic Energy Levels in the Trivalent Lanthanide Aquo Ions. I. Pr3+, Nd3+, Pm3+, Sm3+, Dy3+, Ho3+, Er3+, and Tm3+, The Journal of Chemical Physics 49(10) (1968) 4424-4442. https://doi.org/10.1063/1.1669893.
[32] B.C.G. G. Blasse, Luminescent Materials, Springer Berlin, Heidelberg, 2012, pp. X, 232.
[33] D.L. Dexter, A Theory of Sensitized Luminescence in Solids, The Journal of Chemical Physics 21(5) (1953) 836-850. https://doi.org/10.1063/1.1699044.
[34] Y. Zhang, L. Mei, H. Liu, D. Yang, L. Liao, Z. Huang, Dysprosium doped novel apatite-type white-emitting phosphor Ca9La(PO4)5(GeO4)F2 with satisfactory thermal properties for n-UV w-LEDs, Dyes and Pigments 139 (2017) 180-186. https://doi.org/https://doi.org/10.1016/j.dyepig.2016.11.011.
[35] A. Cadiau, C.D.S. Brites, P.M.F.J. Costa, R.A.S. Ferreira, J. Rocha, L.D. Carlos, Ratiometric Nanothermometer Based on an Emissive Ln3+-Organic Framework, ACS Nano 7(8) (2013) 7213-7218. https://doi.org/10.1021/nn402608w.
[36] E.J. McLaurin, L.R. Bradshaw, D.R. Gamelin, Dual-Emitting Nanoscale Temperature Sensors, Chemistry of Materials 25(8) (2013) 1283-1292. https://doi.org/10.1021/cm304034s.
[37] H. Zou, X. Yang, B. Chen, Y. Du, B. Ren, X. Sun, X. Qiao, Q. Zhang, F. Wang, Thermal Enhancement of Upconversion by Negative Lattice Expansion in Orthorhombic Yb2W3O12, Angewandte Chemie International Edition 58(48) (2019) 17255-17259. https://doi.org/10.1002/anie.201910277.
[38] X. Zhang, Y. Huang, M. Gong, Dual-emitting Ce3+, Tb3+ co-doped LaOBr phosphor: Luminescence, energy transfer and ratiometric temperature sensing, Chemical Engineering Journal 307 (2017) 291-299. https://doi.org/10.1016/j.cej.2016.08.087.
[39] X. Min, Z. Huang, M. Fang, Y.-G. Liu, C. Tang, X. Wu, Energy Transfer from Sm3+ to Eu3+ in Red-Emitting Phosphor LaMgAl11O19:Sm3+, Eu3+ for Solar Cells and Near-Ultraviolet White Light-Emitting Diodes, Inorganic Chemistry 53(12) (2014) 6060-6065. https://doi.org/10.1021/ic500412r.
[40] X. Min, M. Fang, Z. Huang, Y.g. Liu, C. Tang, H. Zhu, X. Wu, Preparation and luminescent properties of orange reddish emitting phosphor LaMgAl11O19:Sm3+, Optical Materials 37 (2014) 110-114. https://doi.org/https://doi.org/10.1016/j.optmat.2014.05.008.
[41] A. Kumar, J. Manam, Enhancement of dual-mode emission and temperature sensing performance in Y2Zr2O7: Er3+ nano phosphor by incorporation of lithium ions, Ceramics International 48(10) (2022) 13615-13625. https://doi.org/https://doi.org/10.1016/j.ceramint.2022.01.241.

[42] L. Lei, D. Chen, C. Li, F. Huang, J. Zhang, S. Xu, Inverse thermal quenching effect in lanthanide-doped upconversion nanocrystals for anti-counterfeiting, Journal of Materials Chemistry C 6(20) (2018) 5427-5433. https://doi.org/10.1039/c8tc01433g.
[43] X.Y. Zhang, G.T. Pang, G.C. Xing, R. Chen, Temperature dependent optical characteristics of all-inorganic CsPbBr3 nanocrystals film, Materials Today Physics 15 (2020). https://doi.org/10.1016/j.mtphys.2020.100259.
[44] V. Chauhan, P. Dixit, P.K. Pandey, S. Chaturvedi, P.C. Pandey, Dy3+-Assisted Negative-Thermal Quenching in Ho3+-Doped SrMoO4 for Luminescence Thermometry and Lighting Applications, The Journal of Physical Chemistry C 127(38) (2023) 19159-19171. https://doi.org/10.1021/acs.jpcc.3c03710.
[45] S. Ling, X. Qin, Y. Yan, C. Chen, K. Meng, J. Ming, S. Liao, Y. Huang, L. Hou, Crystal defect induced zero thermal quenching β-NaYF4: Eu3+, Sm3+ red-emitting phosphor, RSC Advances 13(1) (2023) 534-546. https://doi.org/10.1039/d2ra06567c.